Princeton Optronics

is now

Member of the ams Group

The technical content of this Princeton Optronics document is still valid.

Contact information:

Headquarters:
ams AG
Tobelbader Strasse 30
8141 Premstaetten, Austria
Tel: +43 (0) 3136 500 0
e-Mail: ams_sales@ams.com

Please visit our website at www.ams.com

Two-dimensional pseudo-random optical phased array based on tandem optical injection locking of vertical cavity surface emitting lasers

Keyvan Sayyah,[1,*] Oleg Efimov,[1] Pamela Patterson,[1] James Schaffner,[1] Carson White,[1] Jean-Francois Seurin,[2] Guoyang Xu,[2] and Alexander Miglo[2]

[1]*HRL Laboratories, 3011 Malibu Canyon Road, Malibu, CA 90265, USA*
[2]*Princeton Optronics, 1 Electronics Dr.,Trenton, NJ 08619, USA*
[*]*sayyah@hrl.com*

Abstract: We demonstrate, both theoretically and experimentally, a pseudo-random, two-dimensional optical phased array (OPA) concept based on tandem injection locking of 64-element vertical cavity surface emitting laser (VCSEL) arrays. A low cavity-Q VCSEL design resulted in an injection locking optical power of less than 1 μW per VCSEL, providing large OPA scaling potential. Tandem injection locking of two VCSEL arrays resulted in measured controllable optical phase change of 0-1.6π. A high quality beam formed with suppressed grating lobes due to the pseudo-random array design was demonstrated with performance close to simulated results. A preliminary 2.2° x 1.2° beam steering example using the tandem arrays was also demonstrated.

OCIS codes: (140.2010) Diode laser arrays; (140.3298) Laser beam combining; (140.7260) Vertical cavity surface emitting lasers; (140.3520) Lasers, injection-locked.

References and links

1. P. F. McManamon, P. J. Bos, M. J. Escuti, J. Heikenfeld, S. Serati, H. Xie, and E. A. Watson, "A review of phased array steering for narrow-band electrooptical systems," IEEE Proc. **97**, 1078–1096 (2009).
2. J. E. Kansky, C. X. Yu, D. V. Murphy, S. E. J. Shaw, R. C. Lawrence, and C. Higgs, "Beam control of a 2D polarization maintaining fiber optic phased array with high-fiber count," Proc. SPIE **6306**, 63060G (2006).
3. F. Aflatouni and H. Hashemi, "An electronically controlled semiconductor laser phased array," in *IEEE MTT-S International Microwave Symposium Digest* (IEEE, 2012), pp. 1–3.
4. B.-W. Yoo, M. Megens, T. Chan, T. Sun, W. Yang, C. J. Chang-Hasnain, D. A. Horsley, and M. C. Wu, "Optical phased array using high contrast gratings for two dimensional beamforming and beamsteering," Opt. Express **21**(10), 12238–12248 (2013).
5. J. Sun, E. Timurdogan, A. Yaacobi, E. S. Hosseini, and M. R. Watts, "Large-scale nanophotonic phased array," Nature **493**(7431), 195–199 (2013).
6. J. K. Doylend, M. J. R. Heck, J. T. Bovington, J. D. Peters, L. A. Coldren, and J. E. Bowers, "Two-dimensional free-space beam steering with an optical phased array on silicon-on-insulator," Opt. Express **19**(22), 21595–21604 (2011).
7. G. Hergenhan, B. Lücke, and U. Brauch, "Coherent coupling of vertical-cavity surface-emitting laser arrays and efficient beam combining by diffractive optical elements: concept and experimental verification," Appl. Opt. **42**(9), 1667–1680 (2003).
8. C. A. Balanis, *Antenna Theory Analysis and Design*, 2nd ed. (John Wiley & Sons, 1997).
9. F. Mogensen, H. Olesen, and G. Jacobsen, "Locking conditions and stability properties for a semiconductor laser with external light injection," IEEE J. Quantum Electron. **21**(7), 784–793 (1985).
10. B. Lucke, G. Hergenhan, U. Branch, and A. Giesen, "Phase tuning of injection-locked VCSELs," IEEE Photonics Technol. Lett. **13**(2), 100–102 (2001).
11. J. T. Verdeyen, "Laser Electronics," 3rd ed. (Prentice Hall, 1995), Ch. 6.
12. W. Zeller, M. Kamp, and J. Koeth, "High power DFB laser diodes," Proc. SPIE **7583**, 75830R1 (2010).

1. Introduction

Electronically addressable optical phased arrays (OPA) with scalable output power and fast beam steering capability have been a long-sought-after technology for a myriad of

#240191 Received 6 May 2015; revised 7 Jul 2015; accepted 7 Jul 2015; published 17 Jul 2015

applications such as scanning laser radar (LADAR) for 3D mapping and surveillance, free-space laser communication, target detection and designation, and missile countermeasures, to name a few. Unlike microwave and millimeter wave phased arrays, realization of OPAs is much more difficult due to the small inter-element spacing (on the order of λ) required for optical phased arrays, owing to the short wavelength of light.

Despite this difficulty, many approaches to demonstrate optical phased arrays have been attempted. The oldest optical beam steering approach is based on liquid crystal (LC) diffractive and refractive elements or arrays, which use the large refractive index change in LCs to obtain the required optical phase change [1]. This well-developed approach has the advantages of having a rather simple architecture and low power consumption. On the other hand, the beam steering speed is slow (~10 ms and 2 ms for diffractive and refractive LC devices, respectively) due to the mechanical motion of the LC molecules. Also, the diffraction efficiency degrades at larger steering angles.

Two-dimensional arrays of fiber-based optical amplifiers in standard master oscillator-power amplifier (MOPA) architecture have also been developed for optical beam forming and control. The optical components for this approach are well developed in the near-IR band (0.8-1.6 μm), with as many as 48 fiber amplifiers in an array with a pitch of 250 μm coherently combined via individual all-fiber optical phase modulators [2]. However, it is difficult to scale up this phased array to large number of elements (>100), it has a low fill-factor, and the system is too bulky and expensive for many applications.

Yet another approach is the coherent combination of semiconductor lasers using optical phase-lock loops (OPLL). In this approach, phase modulation for each element of the array is controlled by a corresponding RF phase modulator and an optoelectronic phase lock-loop. Consequently, there is no need for optical phase modulators which results in some system simplification. However, unless the OPLL circuitry for each element is fully integrated (including the lasers and photodetectors) and arrayed with a small inter-element spacing, this approach is not amenable to large scaling. So far, only a 2-element array has been demonstrated [3].

Some recent promising approaches include a two-dimensional array of micro-electromechanical (MEMS) phase shifters, a nanophotonic-based 2-D phased array, and a linear array of semiconductor-based optical amplifier (SOA), phase modulators, and gratings. The MEM-based OPA consists of a two-dimensional array of broadband and high contrast grating (HCG) micromirrors with a piston-like motion for controllable phase modulation. One of the advantages of this approach is the use of a Si MEMS-compatible fabrication process which is amenable to large scaling. Also, the grating-based micromirrors have a low enough mass to enable microsecond-scale phase modulation. In this approach, however, the laser source is off-chip and is coupled to the MEMS phase shifting array via free-space optics which results in some optical loss. An 8x8 array with ± 1.28° beam steering has been demonstrated [4].

The nanophotonic OPA is based on a two-dimensional array of Si photonic directional coupler splitters, thermo-optic phase modulators, and grating outcouplers [5]. This approach is highly compatible with standard CMOS processing, and is scalable to a very large number of 2D elements. Indeed, a 64x64 element static array has already been demonstrated. However, the architecture results in some optical loss in the phase modulators and grating structures, which reduces the overall OPA efficiency. Furthermore, the thermo-optic phase modulators limit the OPA steering speed (~1 ms), and consume additional power (~17 mW per element for 2π phase shift) in addition to that dissipated by the off-chip laser source .

The linear array of SOAs, phase modulators and gratings together with a master laser is a fully-integrated semiconductor based MOPA architecture. It is a scalable *quasi*-2D OPA approach since the beam steering in the direction parallel to the linear array is not controlled by phase modulation, but rather by tuning the wavelength of the master laser, which in turn results in a change in the outcoupling angle of the grating. This feature, indeed, is the main

#240191 Received 6 May 2015; revised 7 Jul 2015; accepted 7 Jul 2015; published 17 Jul 2015

disadvantage of this approach which limits the steering angle of the device (<10°) due to the limited wavelength tuning range of the master laser. An 8-element linear array, using heterogeneously integrated InP-based master laser and SOAs, with Si based thermo-optic phase modulators has been demonstrated with ± 6° beam steering in the direction perpendicular to the linear array [6]. In this approach the thermo-optical modulators can be replaced with electro-optic or current injection/depletion semiconductor phase modulators for fast steering speeds (<1μs).

Finally, there has been a demonstration of a single injection-locked periodic VCSEL array, with a pitch of 250 μm, for coherent optical beam combing [7]. In this work, the output light of one VCSEL element on the edge of the array is extracted and collimated using appropriate optics to injection lock the remaining VCSELs. Furthermore, a microlens array is positioned on top of the VCSEL array in order to effectively increase the array fill-factor for improved beam combining efficiency. This VCSEL-based OPA architecture is not suitable for beam steering since the presence of the collimating microlens array results in a very narrow field-of-view (<0.25°) for each array element. Without the collimating microlens array, the large inter-element spacing of 250 μm for the periodic VCSEL array will result in a very inefficient OPA, with strong gating lobes in its field-of-view at different scan angles (very low power in the main lobe of the formed beam). Also, the maximum phase modulation available with a single level of injection locking is ≤π, hence precluding proper phased array operation for beam forming and steering.

In this paper, we introduce a novel two-dimensional pseudo-random optical phased array architecture based on *the tandem injection locking* of two 64-element VCSEL arrays arranged in a *pseudo-random* element placement. This approach is an electronically controlled 2D optical phased array with *integrated sources* in which the pseudo-random arrangement of the array elements eliminates the grating lobes that are present in the periodic arrays described above. We demonstrate beam forming and steering through the control of the optical phase of each emitting element via detuning of the VCSEL current in its injection locked state. This approach eliminates the need for external optical phase modulators, hence reducing the OPA complexity. Also, since there are no additional optical elements above the emitting VCSELs, the optical efficiency for this OPA approach is very high. Finally, the fast current-tuned modulation speed of the VCSELs enables ns-scale optical beam forming and steering.

2. Pseudo-random VCSEL array design and fabrication

Figure 1(a) shows the schematic of the novel 2D OPA architecture composed of 2 tandem injection-locked pseudo-random VCSEL arrays. A single master laser injection locks the first pseudo-random VCSEL array, which, in turn, locks a second identical array. As shown in Section 3 below, a small tuning of the VCSEL drive current in the injection-locked regime results in up to nearly π-radian optical phase change, while the VCSEL maintains its coherence with the optical injection source (master laser). Figure 1(b) shows the layout of the 64-element pseudo-random 2D VCSEL arrays used in this work. Each VCSEL mesa has a diameter of 19 μm, with a 3 μm wide Au metal line connecting the VCSEL p-side contact to its corresponding pad on the chip periphery. The minimum spacing between VCSELs in this design is 30 μm, and the overall size of the array is constrained to an area of 300x300 μm^2.

Periodic phased arrays with element spacing larger than a half-wavelength ($\lambda/2$) could have strong far-field grating lobes at angles determined by Eq. (1) below [8]:

#240191 Received 6 May 2015; revised 7 Jul 2015; accepted 7 Jul 2015; published 17 Jul 2015

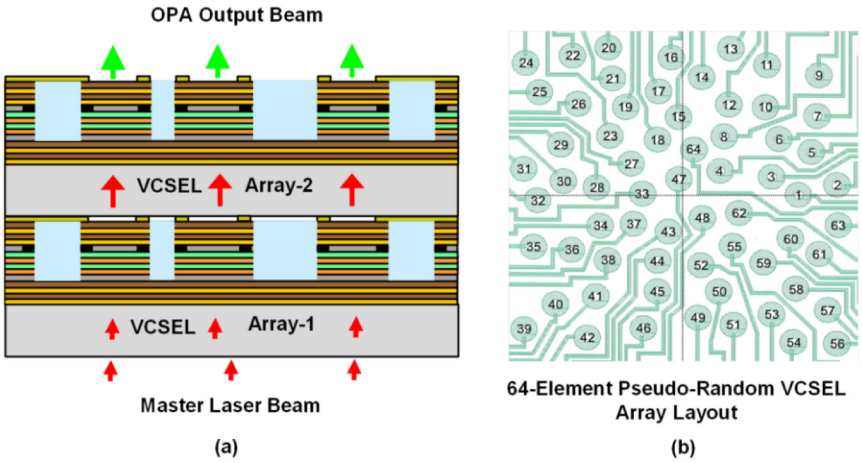

Fig. 1. (a) Schematic of the novel 2D OPA architecture composed of 2 tandem injection-locked VCSEL arrays with a single master laser, and (b) the layout of the 64-element pseudo-random VCSEL array used in this OPA architecture.

$$\mathrm{Sin}\left(\theta_{gl}\right)-\mathrm{Sin}(\theta_0)=\frac{n\lambda}{d} \tag{1}$$

where, θ_0 and θ_{gl} are the steering and grating lobe angles, respectively, d is the array element spacing, and n is an integer. For example, in order to push the grating lobes beyond a maximum steering angle of ± 22.5° (total field-of-view of 45°), an inter-element spacing $d \leq 1.3\lambda$ is required. For an operating wavelength of 1.1 μm, the element spacing d≤1.5 μm, which is difficult to obtain for OPAs.

Figure 2(a) shows the simulated far-field pattern of a 89x89 element periodic phased array with an element spacing of ~21.4 μm, for an overall array dimension of 1900x1900 μm^2, and an element factor with 54° half-angle divergence. Also shown in Fig. 2(a), is the simulated far-field pattern of a pseudo-random array (10 μm minimum element spacing) with about the same number of elements (8000), array dimensions, and elemental divergence angle. Pronounced grating lobes, 3° apart, are clearly visible in the far-field pattern of the periodic array, while they are eliminated in the pseudo-random array. Figure 2(b) shows a close-up view around the central lobe, which is nearly identical for both the periodic and pseudo-random arrays. For the latter, the energy in the eliminated grating lobes is transferred to the noise-like side lobes, with peak levels 30 dB below the intensity of the central lobe for this large array.

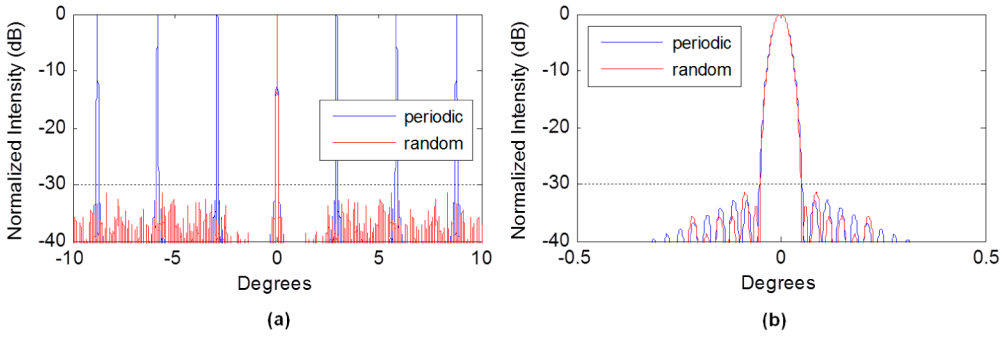

Fig. 2. (a) Comparison of simulated far-field patterns for a 89x89-element periodic and 8000-element pseudo-random phased arrays with identical array dimensions and elemental

#240191 Received 6 May 2015; revised 7 Jul 2015; accepted 7 Jul 2015; published 17 Jul 2015

divergence angle, clearly showing the elimination of the grating lobes in the latter. (b) Close-up view of the central lobe of the two arrays, indicating almost identical patterns.

The VCSEL structure used here, which emitted at a nominal wavelength of 1064 nm, was based on a lower cavity-Q design in which the top and bottom distributed Bragg reflector (DBR) mirrors have lower reflectivities compared to conventional VCSEL designs in order to enable transmission of injection locking light from the master laser through its back mirror. The main fabrication steps of the VCSEL arrays, following the growth of the DBR mirrors and the quantum well layers on n-GaAs wafers, involved: (1) forming the p-type metal contact ring, (2) etching the VCSEL mesa, (3) depositing a passivation layer on the VCSEL array, (4) forming the metal interconnect lines from the p-contact ring to the contact pads on the chip periphery, (5) thinning the substrate (~100 μm), and (6) forming the n-metal contact on the substrate backside with open apertures (20 μm) that are aligned with each VCSEL for the transmission of the injection locking light. Figure 3 shows a scanning electron micrograph (SEM) of a typical 64-element pseudo-random VCSEL array following the completion of the processing steps, with a close-up view of one selected VCSEL element and the metal interconnect lines.

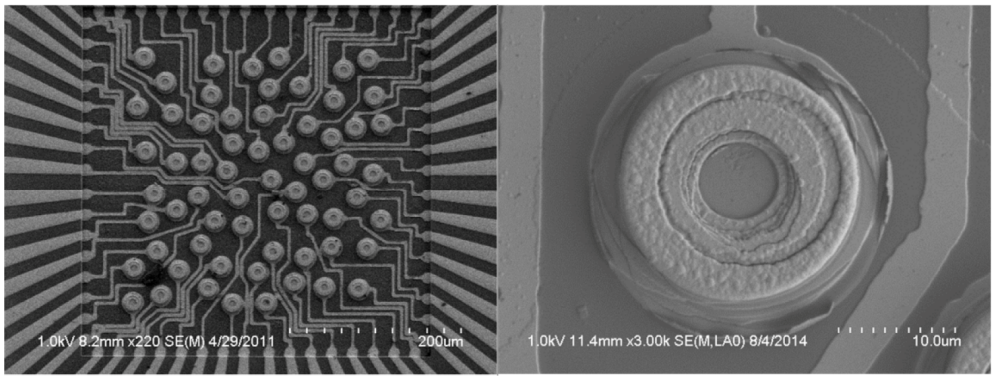

Fig. 3. (left) SEM photomicrograph of a fully processed 64-element pseudo-random VCSEL array showing the metal interconnect lines for each individual VCSEL, and (right) a close-up view of a single VCSEL element showing its mesa structure.

3. Experimental results

One of the main features of this optical phased array approach is that the emitting VCSEL array is the top-most layer in the vertically stacked tandem injection locking scheme, as shown in Fig. 1(a). Thus, this OPA approach has a much higher optical efficiency in comparison with waveguide-based phased arrays in which the waveguide splitting and propagation losses reduce the emitted optical power and OPA efficiency [6].

To this end, we first evaluated the light-current-voltage (LIV) characteristics of the novel low cavity-Q VCSEL before the optical injection locking and beam forming experiments. Figure 4 shows the measured LIV for one such VCSEL, demonstrating single mode output power of up to 4 mW, with side-mode suppression ratio (SSR) of 35 dB at an emitting wavelength of 1064.4 nm. Also shown in Fig. 4(a) is the VCSEL backside emitting light level as a function of the drive current. We measured a ratio of 2.43 mW/0.52 mW for the forward/backward emitting light levels at a drive current of 5.25 mA, which is very close to the simulated ratio of 2.43 mW/0.57 mW, hence verifying the accuracy of our VCSEL simulation code.

#240191 Received 6 May 2015; revised 7 Jul 2015; accepted 7 Jul 2015; published 17 Jul 2015

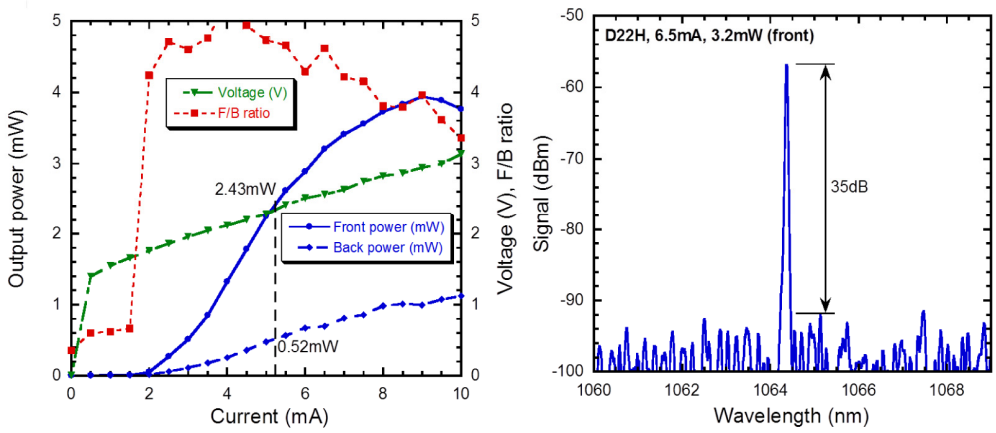

Fig. 4. (a) Measured LIV curves of a typical low cavity-Q VCSEL for both forward and backward emitting light, and (b) optical spectrum of the single mode VCSEL emission with a side mode suppression ratio of 35 dB.

Figure 5 shows the schematic of the optical setup we used for the evaluation of the tandem injection locked VCSEL optical phased array. It consisted of a nominal 1064 nm distributed Bragg reflector (DBR) master laser whose output light was collimated into a 2 mm diameter ($1/e^2$) beam that illuminated the backside of the first 64-element pseudo-random VCSEL array. The 64 emitting beamlets of the first VCSEL array was 1:1 imaged onto the backside of the second identical VCSEL array for injection locking the VCSEL elements in this array. An optical isolator was placed in between the two arrays in order to prevent the backward emitting light from the second array to interfere with the injection locking of the first array. A small fraction (<10%) of the collimated master laser light was split from the main beam and used as a reference beam to form 64 near-field interference patterns with the output beamlets of the second VCSEL array, once both VCSEL arrays were locked to the master laser. The shifting of the fringes of these interference patterns, detected using a high resolution (1800x1200 element) CCD camera, was used to measure the relative phase change of each emitting VCSEL element as a function of the drive currents of the two corresponding injection locked VCSELs in the two arrays. The far-field pattern of the beam formed was recorded using a second CCD camera. An optical fiber mounted on a motorized 2-D translation stage (not shown in Fig. 5) was used to detect the wavelength of the emitting VCSELs using a high resolution (0.02 nm) optical spectrum analyzer.

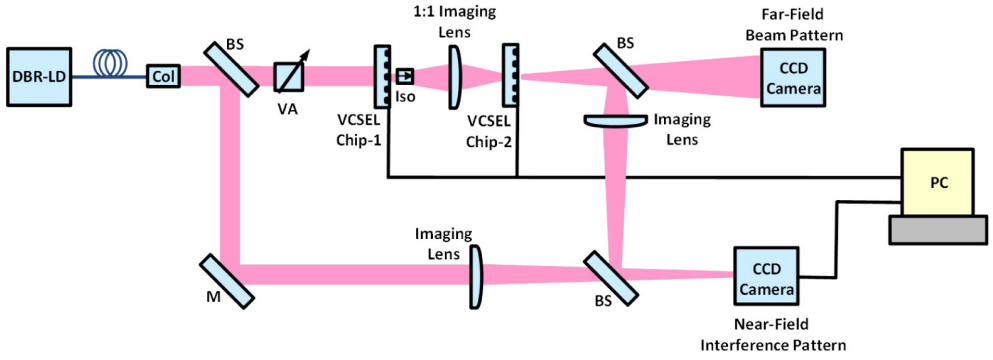

Fig. 5. Schematic of the optical setup used for the evaluation of the tandem injection locked VCSEL-based optical phased array. A CCD camera was used for the detection of the near-field interference fringes for each set of injection locked VCSELs from which their relative optical phase was measured. Another CCD camera was used to record the far-field pattern of the

#240191 Received 6 May 2015; revised 7 Jul 2015; accepted 7 Jul 2015; published 17 Jul 2015

formed optical beam. DBR-LD: distributed Bragg reflector laser diode, Col: fiber collimator, VA: variable attenuator, BS: beam splitter, Iso: optical isolator.

Figure 6 shows the interference fringe patterns of 60 injection locked VCSELs in a 64-element pseudo-random array. The formation of the fringe pattern for each VCSEL is a confirmation that it has been injection locked to the master laser. Stable locking was achieved with optical power levels of < 0.5 μW injected into the 4 μm optical aperture of each VCSEL, which translates to a ratio of injection to emission power levels of $<2x10^{-4}$. Although the maximum free-running wavelength spread of the VCSELs in this array was ~1.2 nm, we were able to injection lock all 60 working VCSELs by adjusting their drive currents in an iterative fashion. We measured a wavelength shift with drive current of ~1 nm/mA at a typical drive current range of 5-7 mA for the low cavity-Q VCSELs used in this work.

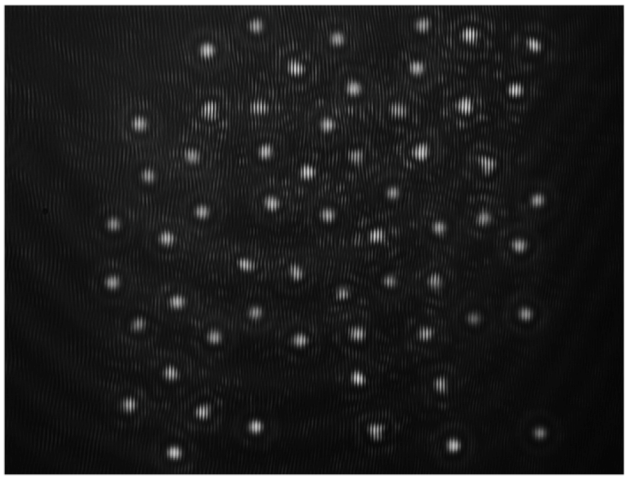

Fig. 6. Interference fringe patterns of 60 injection locked VCSELs in a 64-element pseudo-random array detected using a high resolution CCD camera.

Once the VCSELs were injection locked, they remained locked for tens of minutes even without any implementation of temperature control capability in the device package. This indicates the stability of the low cavity-Q VCSEL injection locking mechanism. Figure 7(a) illustrates the measured phase change of an injection locked VCSEL switched from one extreme edge of the locking range to the other as a function of time. The VCSEL remained locked within the 33 minutes measurement time with a phase drift of <7%.

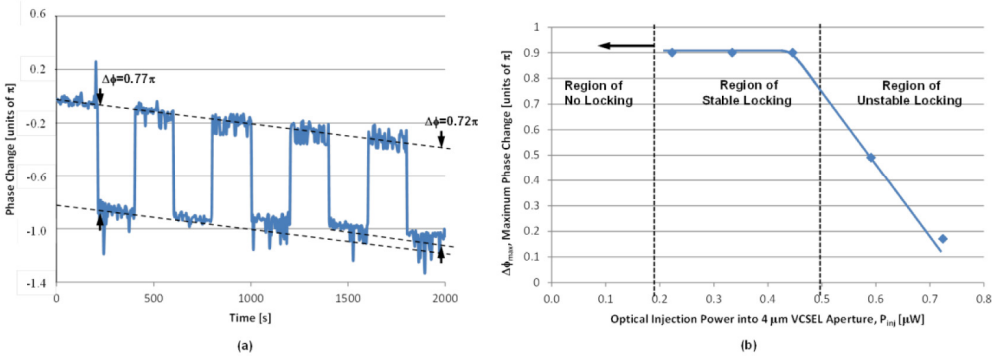

Fig. 7. (a) Measured time dependent phase change of an injection locked VCSEL switched from one extreme edge of the locking range to the other, indicating a phase drift of <7% within the 33 minutes of measurement time. (b) Measured maximum phase change of injection locked VCSEL as a function of the injection light power level, showing 3 regimes of locking.

#240191 Received 6 May 2015; revised 7 Jul 2015; accepted 7 Jul 2015; published 17 Jul 2015

Figure 7(b) shows the measured dependence of the injection locked VCSEL maximum phase change on the injection light power level, P_{inj}, in which three distinct regimes are observed: (1) P_{inj} <0.2 μW, where injection locking is not possible, (2) 0.2 μW <P_{inj} <0.5 μW, is the stable locking region in which a maximum phase change of close to π-radians is achievable, and (3) P_{inj} >0.5 μW, in which the VCSEL enters the dynamically unstable locking region where both the locking bandwidth and maximum available phase change within the locking bandwidth are reduced with increasing level of the injection light level [9].

The locking half-bandwidth, $\Delta f_{L,}$ of an injection locked laser is given by [10]:

$$\Delta f_L = \pm \frac{1-R}{2\pi\pi_{rt}} \sqrt{1+\alpha^2} \sqrt{\frac{P_{inj}}{P_0}} \tag{2}$$

where, R is the effective reflectivity of the VCSEL cavity mirrors, τ_{rt} is the photon round trip time in the laser cavity, α is the linewidth enhancement factor, and P_{inj} and P_0 are the VCSEL injection and output power levels, respectively. Furthermore, $\frac{1-R}{\tau_{rt}} = \frac{1}{\tau_p}$, where τ_P is the photon lifetime, and $R = \sqrt{R_f R_b}$ with R_f and R_b denoting the VCSEL front and back facet DBR mirror reflectivities [11]. For the low cavity-Q VCSEL structure used in this work, R = 0.9888, τ_p ~3.7 ps, τ_{rt} ~41.5 fs and α = 4.1 [10]. Thus for P_{inj} = 0.5 μW and P_0 = 2.5 mW, the VCSEL locking bandwidth $2\Delta f_L$~5.1 GHz.

For the injection locked VCSELs used in this work, we have measured current excursions on the order of ~15-20 μA in the injection locking region, which coupled with the VCSEL current dependent wavelength tuning of $\Delta\lambda/\Delta I$ = 1 nm/mA, results in measured locking bandwidths of ~4.0-5.3 GHz at 1064 nm wavelength. This is in relatively good agreement with the computed locking bandwidth discussed above. With the current control (resolution) of 0.5 μA available in the VCSEL driver electronics used in this work, we were able to achieve >30 independent optical phase values (~5 bits) per element for our injection locked VCSEL-based optical phased array.

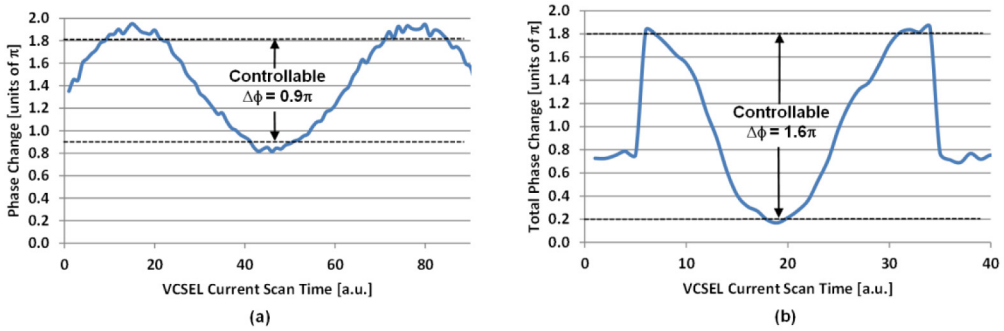

Fig. 8. (a) Measured phase change of the first VCSEL in the tandem injection locking arrangement for an applied linear sawtooth current waveform shown in the inset. (b) Measured phase change of the output VCSEL in the tandem injection locking configuration for the synchronized linear ramp drive current waveforms applied to the two VCSELs, as shown in the inset.

Figure 8 shows the measured phase change of a pair of tandem injection locked VCSELs as a function of the scanned VCSEL drive current. In Fig. 8(a), the phase change of the first VCSEL in the tandem injection locking arrangement, which is locked by the master laser, is shown for a linear sawtooth VCSEL drive current waveform. As the measurement shows, a controllable phase change with a maximum value of ~0.9π is demonstrated using the interferrometric phase measurement technique described above. The dashed horizontal lines

#240191 Received 6 May 2015; revised 7 Jul 2015; accepted 7 Jul 2015; published 17 Jul 2015

in Fig. 8(a) show the two edges of the injection locking band in which the locked VCSEL is coherent with the master laser. Figure 8(b) shows the measured phase change of the output VCSEL in the tandem injection locking configuration in which the master laser locks the first VCSEL, whose emitted light in turn locks the second (output) VCSEL. For this measurement, two synchronized sawtooth drive current waveforms are applied to the two tandem injection locked VCSELs. The ramp current of the first VCSEL scans the phase of this locked VCSEL between the two edges of its locking band (~0.9π phase change), while the second locked VCSEL is at the leading edge of its locking band. At this point, the first VCSEL is maintained at the trailing edge of its locking band, while the drive current of the second VCSEL is linearly ramped to its trailing edge for an additional phase change of ~0.7π, resulting in a total phase change of ~1.6π for the tandem injection locking arrangement, as demonstrated in Fig. 8(b).

In an ideal phased array, phase control of 0-2π for each element is required for optimum operation. However, a more limited phase control in the range of 0-1.5π results in very small degradation in the quality of the formed beam, or the misalignment of the beam pointing direction. Figure 9 shows the simulated far-field patterns of a 5° steered beam for a 64-element pseudo-random phased array with an ideal 0-2π phase control range compared with an identical array in which the phase control is limited to a range of 0-1.5π. In this simulation, the phase of the elements falling in the forbidden 0.5π zone for this generated beam is randomly folded back to the allowed optical phase range. This phase control limitation results in a loss of only 0.16 dB for the main lobe intensity, and a maximum side-lobe level change from −10.23 dB to −9.67 dB.

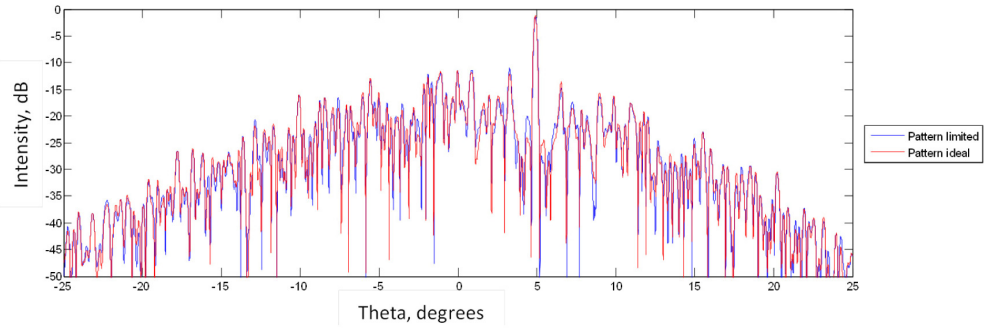

Fig. 9. Comparison of simulated far-field patterns of a beam steered at 5°for a 64-element pseudo-random phased array with an ideal 0-2π phase control compared to an identical one with a more limited 0-1.5π phase control. This phase control limitation results in only 0.16 dB loss of the main lobe intensity and 0.56 dB increase in side-lobe level

Figure 10(a) shows the measured far-field pattern of the pseudo-random optical phased array with a single beam formed using 50 injection-locked VCSELs. As expected, no significant grating lobes are present in the far-field pattern due to the randomness of the array architecture. However, a side-lobe pattern with a maximum level of −7.0 dB relative to the main beam intensity is present in the far-field image. The VCSELs were driven at an average drive current of 5 mA, resulting in a total emitted power of 125 mW (~2.5 mW per VCSEL), with 30 mW (24%) of this power in the formed beam. It should be noted that output power of the VCSELs in the locked state is the same as in their free-running configuration.

#240191 Received 6 May 2015; revised 7 Jul 2015; accepted 7 Jul 2015; published 17 Jul 2015

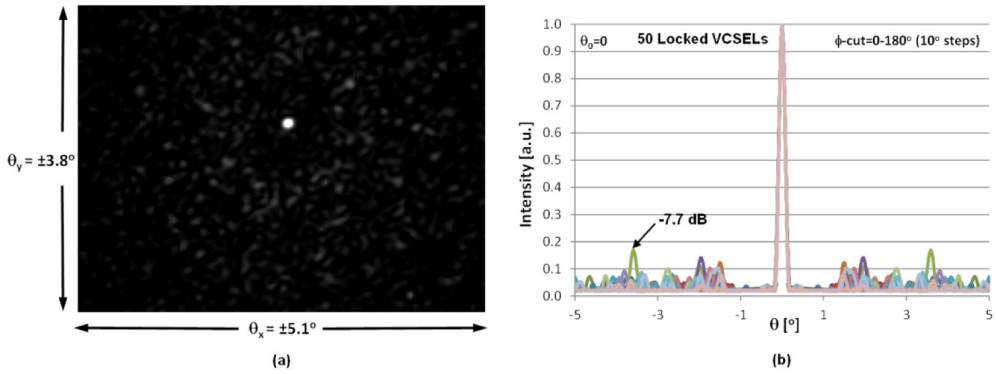

Fig. 10. (a) Measured far-field image of a beam formed using a 50-element injection-locked pseudo-random VCSEL array demonstrating a minimum side-lobe suppression value of 7.0 dB, with no grating lobes. (b) Simulated one-dimensional far-field pattern of the same array measured in (a) for 18 azimuthal direction cuts, showing a minimum side-lobe suppression value of 7.7 dB, in good agreement with the corresponding measured value.

The simulated one-dimensional (Intensity vs. elevation direction, θ) far-field pattern of this 50-element phase locked pseudo-random array is shown in Fig. 10(b) for 18 slices in the azimuthal ϕ-direction, with each cut separated by 10° for a total of 180° in the hemispherical space. The maximum simulated side-lobe level is –7.7 dB relative to the main lobe intensity for a phased array field-of-view of $-5° \leq \theta \leq 5°$, in good agreement with the experimental result indicated above. The measured beamwidth was ~0.31°, which is very close to the theoretical beamwidth of 0.32° extracted from the simulated beam shown in Fig. 10(b).

Finally, Fig. 11 shows an example of 2D electronic steering of a beam formed using 16 pairs of VCSELs in two tandem injection locked pseudo-random VCSEL array. In this demonstration, the main beam formed was steered by 2.2° and 1.2° in the vertical and horizontal directions, respectively, with the appropriate tuning of the drive current, and hence the optical phase of the tandem injection locked VCSELs within the injection locking band. The 16 VCSELs in this demonstration were also driven at an average drive current of ~2.5 mA, resulting in a total emitted power of 40 mW, with ~10 mW (24%) in the steered beam.

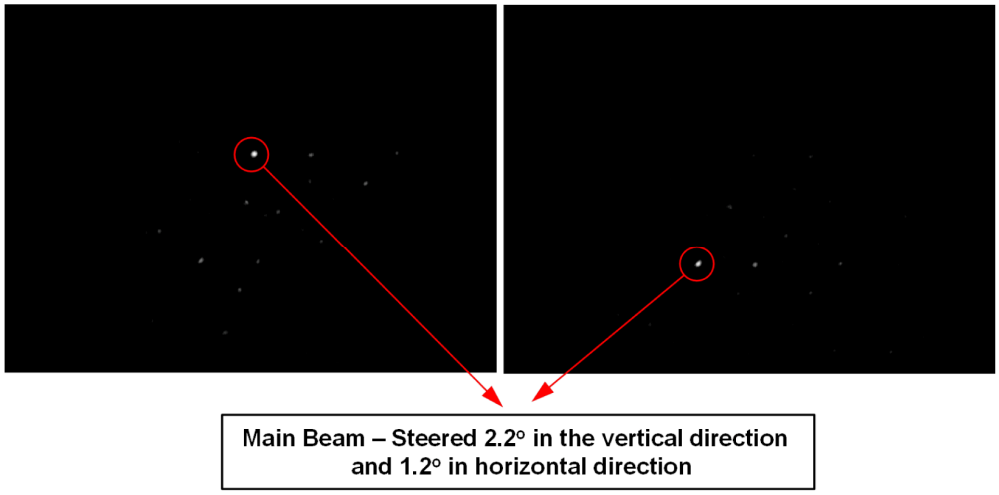

Fig. 11. Electronic steering of 2.2° x 1.2° demonstrated with 16 pairs of VCSELs in two tandem injection locked pseudo-random VCSEL arrays.

#240191 Received 6 May 2015; revised 7 Jul 2015; accepted 7 Jul 2015; published 17 Jul 2015

4. Power scaling of the injection-locked VCSEL optical phased array

The 2-dimensional nature of the injection-locked VCSEL optical phased array approach described in this paper provides a convenient path for power scaling of the array via increasing the number of emitting VCSEL elements. To this end, we analyze here the power scaling efficiency of this OPA approach. Figure 12 shows the schematic of an ultimate vertically integrated optical phased array with two tandem injection-locked pseudo-random VCSEL arrays and a laser diode coupled to a grating outcoupler structure which provides a single collimated vertically emitting master laser light for injection locking. A microlens array is also integrated within the structure in order to increase the coupling efficiency between the master laser and the first injection-locked VCSEL array.

The power scaling capability of the vertically integrated VCSEL-based OPA is driven by the optical power level of the single mode master laser diode, P_{LD}, and various optical coupling inefficiencies, which can be analytically expressed as:

$$P_{LD} = N_{el} P_{inj} / (FF \eta_{\mu L} \eta_{LC} \eta_{OC}) \quad (3)$$

where, η_{el} is the number of scaled array elements, *FF* is the pseudo-random optical phased array and microlens array fill-factor, $\eta_{\mu L}$ is the microlens to VCSEL element coupling efficiency, η_{LC} is the laser diode to grating outcoupler coupling efficiency, and η_{OC} is the grating outcoupling efficiency. Thus for nominal parameters in Eq. (3) of *FF* = 0.3, $\eta_{\mu L}$ = 0.8, η_{LC} = 0.5, and η_{OC} = 0.8, a modest laser diode single mode optical power level of ~50 mW is required to scale the optical phased array to 10,000 elements using the measured injection light level of P_{inj} = 0.5 μW for injection locking each VCSEL element of the array. This modest level of the required master laser diode optical power is mainly due to the very low injection locking light level that results from using the low cavity-Q VCSELs in the 2-dimensional optical phased array. Both distributed Bragg reflector (DBR) and distributed feedback (DFB) laser diodes can readily provide >50 mW of single mode optical power [12].

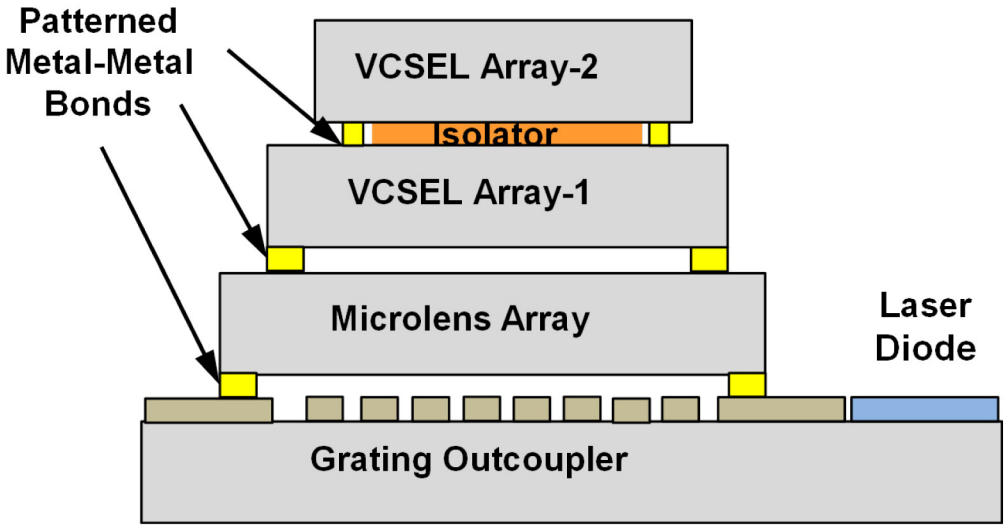

Fig. 12. Schematic of a vertically integrated optical phased array with tandem injection locked VCSEL arrays, a master laser diode coupled to a grating outcoupler providing the master injection light beam, and a microlens array for efficient coupling of the master laser beam to the first VCSEL array.

#240191 Received 6 May 2015; revised 7 Jul 2015; accepted 7 Jul 2015; published 17 Jul 2015

5. Conclusion

We developed and demonstrated a new optical phased array approach for beam forming and steering using tandem injection locking of 64-element pseudo-random VCSEL arrays with a low-cavity Q design. We demonstrated >1.5π phase control using the tandem injection locking approach without the use of an optical phase modulator array. The low-cavity Q VCSEL design resulted in stable optical injection locking over tens of minutes, without any temperature control, using a master laser transmitted through the backside DBR mirror of the VCSEL structure with optical injection power levels of <0.5 μW per VCSEL.

We formed far-field beams with high stability and reproducibility using a pseudo-random array of 50 injection locked VCSELs with measured grating lobe suppression value of 7 dB and beamwidth of 0.3°, very close to the theoretical values. We also demonstrated an example 2.2°x1.2° 2D optical beam steering using 16 pairs of VCSELs in two tandem injection locked VCSEL arrays by controlling the optical phase of the injection locked VCSELs via their drive current tuning within the injection locked regime.

This optical phased array concept is highly scalable due to the 2D nature of the VCSEL array, and the very low optical injection power levels required per element. We projected that scaling to a 10,000 element array requires a master laser power level of ~50 mW, which is readily available via conventional DBR and DFB laser diodes. With 2.5 mW output power per VCSEL, a 10,000 element array will emit a total optical power of 25 W. Assuming a field-of-view of 4° (maximum steering angle of ± 2°), the estimated power in the formed beam is 6W (~24%) with an average element spacing of 30λ used in this phase array.

Acknowledgements

The authors thank Chuni Ghosh from Princeton Optronics, Scott Rodgers, formerly from the Defense Advanced Research Projects Agency, and Weimin Zhou of the Army Research Laboratory for many helpful discussions. This research was supported by the Defense Advanced Research Projects Agency Short-range Wide-field-of-view Extremely-agile Electronically-steered Photonic EmitteR (SWEEPER) program (contract number: HR0011-10-C-0150). The views, opinions, and/or findings contained in this article/presentation are those of the author(s)/presenter(s) and should not be interpreted as representing the official views or policies of the Department of Defense or the U.S. Government.

Approved for Public Release, Distribution Unlimited.

#240191 Received 6 May 2015; revised 7 Jul 2015; accepted 7 Jul 2015; published 17 Jul 2015